Turkish Journal of Electrical Engineering & Computer Sciences

http://journals.tubitak.gov.tr/elektrik/

Research Article

Turk J Elec Eng & Comp Sci
(2017) 25: 2535 – 2546

doi:10.3906/elk-1604-45

A frequency-reconfigurable elliptical monopole antenna for cognitive radio networks

Santasri KOLEY*, **Debjani MITRA**
Department of Electronics Engineering, Indian School of Mines, Dhanbad, India

Received: 04.05.2016 • **Accepted/Published Online:** 20.09.2016 • **Final Version:** 29.05.2017

Abstract: In this paper, an elliptical disk monopole antenna with seven switchable states, including an ultrawideband (UWB) state and six narrowband states, is presented. It consists of an elliptical disk radiator to operate in the UWB mode for cognitive radio (CR) sensing. To operate in the narrowband mode, the antenna is fed through a defected ground structure (DGS) integrated microstrip line. Frequency reconfigurability is achieved by changing the DGS slot length using six electronic switches. The simple proposed design can cover a wide range of frequency bands from 0.75 to 12 GHz, has an omnidirectional radiation pattern with high gain, and is especially suitable as a CR front-end. The fabricated prototype shows good impedance matching in the specified frequency range.

Key words: Cognitive radio, reconfigurable antenna, switchable filter, ultrawideband

1. Introduction

The demand for limited spectrum resources is becoming too large to support various wireless services through traditional fixed frequency allocation. Cognitive radio (CR) systems are envisioned to be a revolutionary concept in overcoming the spectrum scarcity by dynamic spectrum allocation (DSA). In CR networks, secondary users (SUs) are enabled to access unused frequency bands of licensed primary users (PUs) without causing any harmful interference, which leads to remarkable improvements in spectrum efficiency [1]. Ultrawideband (UWB) is a promising technology that meets the requirements of CR networks very well when operating in the "underlay" mode. However, in the "overlay" mode, SUs are allowed opportunistic spectrum access to licensed bands in case they are not used by the PUs at a particular time and frequency. Thus, a CR front-end system requires a UWB antenna for wideband spectrum sensing and another reconfigurable narrowband antenna for communication purposes. In a CR network, an integrated wideband and reconfigurable narrowband antenna is preferable, where wideband is required for UWB spectrum-sensing and narrowband is desired for communication. Antennas are usually tuned by introducing switching techniques such as electronic switches, photoconductive switches, field effect transistor (FET) switches, radio frequency (RF) microelectromechanical systems (MEMS), p-i-n diodes, and varactor diodes.

The literature specifies several antenna designs for sensing CR operations over a wideband. An UWB printed planar elliptical monopole antenna was reported in [1]. The antenna can be used for multiband operation with an omnidirectional radiation pattern in the azimuth plane. The antenna operates over an extremely wide impedance bandwidth in the range of 0.75–20 GHz. A CR reconfigurable multiple-input multiple-output (MIMO) and sensing antenna system was presented in [2]. The proposed sensing antenna is used to cover a

*Correspondence: santasrikoley27@gmail.com

wide range of frequency bands from 720 to 3440 MHz. An UWB compact planar rectangular folded monopole antenna with a bandwidth of 0.5–9 GHz was presented in [3]. A new wideband antenna was proposed in [4] to access a wide range of different entertainment, information, and data transfer services, including Bluetooth, Wi-Fi, GPS, DVB-H, and UWB. The antenna operates from 460 MHz up to frequencies in excess of 10.6 GHz. In [5], a planar disk antenna compatible with cognitive radio was developed to operate from 0.77 to 11.23 GHz. However, these antennas [1–5] are designed for wideband operations and they need to be reconfigured for narrowband operation.

In general, there are two ways to achieve wideband to narrowband reconfiguration. One approach is to place a wideband antenna and a reconfigurable narrowband antenna side by side, using separate excitation ports. A second approach is to reconfigure a single-port wideband antenna into narrowband mode by introducing a filter property in the antenna structure or by switching parts of the structure [6]. In [7], a circular disk monopole was excited with two ports at opposite sides; one CPW feed port was used for wideband-sensing operation and the other port consisted of a microstrip feed line with DGS for narrowband communication operation. The DGS slots act as a bandpass filter that suppresses frequencies outside the desired band, and its operating frequency band can be tuned by varying the length of the slots. In [8], the wideband antenna proposed in [4] was integrated with a narrowband slot antenna. However, the antennas [7,8] were designed for fixed narrowband operation only.

In [9], the antenna structure consisted of a UWB antenna and a switched subband antenna system. Here five different antenna patches were designed within a circular section, which connected each shape at different times with the rotation of the circular section via a stepper motor mounted on the backside. This antenna is able to tune throughout the whole band covered by the sensing antenna (2–10 GHz). The main demerits of these types of structures are their complexity and switching times due to rotational motor implementation. In [10], a photoconductive switch-based antenna was demonstrated to achieve frequency reconfigurability. The antenna comprises two monopoles: one for UWB operation and another in reconfigurable narrowband mode, which are placed in close proximity to one another. The narrowband reconfigurability is achieved by integrating laser diodes within the modified monopole antenna structure in order to control the switching state of photoconductive silicon switches. This scheme has the advantage of eliminating the use of optical fiber cables to guide light to the switches and enables easier integration of the reconfigurable antenna in a complete communication system. The antennas in [11] have two microstrip-fed monopole antennas on the same board and are spaced apart side by side. One of them is an UWB egg-shaped patch-sensing antenna. In the communicating antenna, it has a 1-mm-wide long line connected to the microstrip-fed section. This structure yields multiple resonances in the UWB sensing range due to harmonics. The antenna integration method suggested here may not be considered as truly integrated, as the parts do not occupy the same area.

Dual-port antennas enable simultaneous sensing and communicating over the channel, but they have limitations in terms of their relatively large size and the coupling between the two ports [12]. These limitations are solved by using single-port antennas. In [13], a reconfigurable planar monopole to microstrip patch antenna was proposed only for fixed narrowband operation at 7.64 GHz. In [14], a circular UWB slot antenna, nested with two circular annuli, was proposed to reconfigure the antenna between two wideband modes and one single narrowband mode. In [15], an optically controlled reconfigurable planar monopole antenna was presented to operate at UWB and three narrow bands by controlling four photoconductive switches. Single-port frequency-tunable filter antennas for cognitive radios were proposed in [16–22]. To obtain a narrowband operation, a defected microstrip structure (DMS) bandpass filter was embedded in the feed line of an UWB antenna. In [16],

the filter, incorporated with a varactor diode, was tuned in a frequency range of 4.5–7 GHz. However, in [17], five different narrowband modes were achieved with six idle electronic switches incorporated into the filter. In [18], an open loop resonator-based band-stop filter configuration was used for narrowband operation. An UWB microstrip monopole antenna with reconfigurable multiband function was presented in [19]. Reconfigurability was achieved by using gallium arsenide (GaAs) FET switches to connect multiple stubs of different lengths to the main feed line of the monopole. In [20], a microstrip-fed circular disk UWB monopole was connected through half-wave resonator stubs. In [21], a reconfigurable filter was incorporated into the ground plane of the antenna. In [22], a band reconfigurable monopole antenna was designed in the range of 2.2–6 GHz. Most of these antennas [6–22] are designed for operation above 2 GHz. However, CR antennas must be designed for the lowest frequency below 1 GHz to cover a wide range of licensed frequency bands.

In this paper, a microstrip-fed elliptical UWB monopole antenna is designed for a lowest frequency of 750 MHz to cover most of the frequency bands, including CDMA 800, GSM 900, GSM 1800, GSM 1900, UMTS 2100, WLAN 2.4, WiMAX 3.5, WLAN 5.2, and UWB 3.1–10.6. Several bands in the sub-1 GHz spectrum have been identified for CR application due to digital switchover. The proposed antenna is a good choice for CR application and has a simple structure and the smallest size in comparison to the CR antennas reported in [4,5,7]. By integrating a DGS into the microstrip feed line, the proposed antenna can operate in different frequency reconfigurable narrowband modes to cover the whole sensing bandwidth. To the best of our knowledge, tunability over such a wide frequency range has not been reported for planar monopole antennas. Details of the proposed UWB elliptical monopole antenna design are described in Section 2. Section 3 presents the DGS narrowband filter design. In Section 4, the reconfigurable antenna design is explained. Finally, the conclusion is provided in Section 5.

2. Ultrawideband antenna design

A microstrip-fed elliptical disk monopole antenna is used for UWB operation, as shown in Figure 1. The ellipse has major axis radius a and minor axis radius b, and the separation between the ground plane and ellipse is g. W and L denote the overall antenna dimension. In this study, a low-cost FR4 dielectric substrate with a thickness of 1.6 mm and a relative permittivity of 4.4 is chosen. Therefore, width W_f of the microstrip feed line is fixed at 3 mm for 50Ω matching. The simulations are carried out using CST Microwave Studio, which utilizes a finite integration technique (FIT) for electromagnetic computations.

An elliptical monopole antenna (EMA) is a generalized case of the circular monopole antenna (CMA), wherein the frequency bandwidth improves due to an increase in the ellipticity ratio. The EMA is fed along the major axis through a microstrip line. For calculating a lower frequency corresponding to voltage standing wave ratio (VSWR) = 2 of the planar monopole antennas, the following equation is used [23]:

$$f_L = \frac{72}{2a + b/4 + g} \quad GHz \tag{1}$$

2.1. Effect of ellipticity ratio

The performance of the EMA is compared with the CMA by varying the ellipticity ratio. The simulated return losses are shown in Figure 2 for different combinations of major and minor axes. The first resonance frequency shifted to the lower frequency region by increasing the major axis, whereas the minor axis is reduced to keep the same patch area. Improved VSWR BWs are obtained for the EMA with different ellipticity ratios compared

to the CMA, as given in Table 1. The theoretical f_L obtained using Eq. (1) closely matches the simulation results, where g is taken as 0.5 mm. It is observed that the EMA can resonate below $\lambda/4$ length by increasing the elliptical ratio, where λ is free space wavelength. For an ellipticity ratio of 1.33, the ratio between $(a+b)$ and λ becomes 0.228, which is below $\lambda/4$ length.

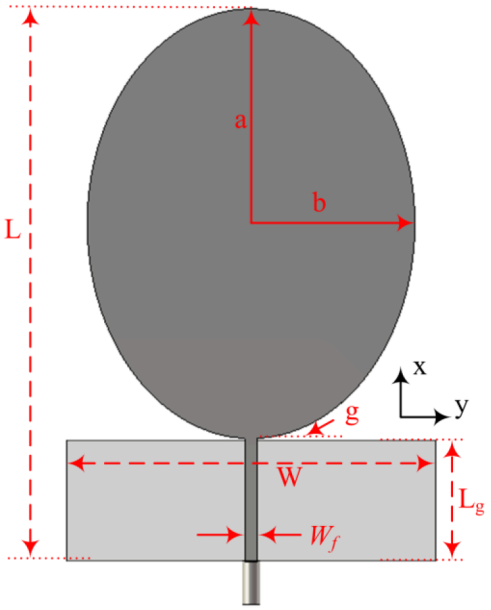

Figure 1. Simulated geometry of microstrip-fed elliptical monopole antenna.

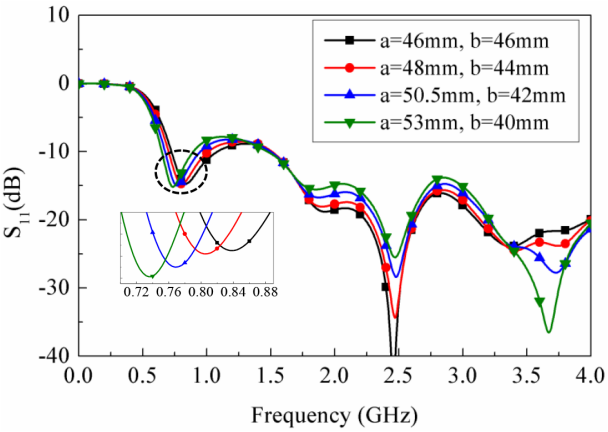

Figure 2. Simulated return loss curves for different axis combinations where the other parameters are $L = 150$ mm, $W = 180$ mm, $L_g = 34.5$ mm, and $g = 0.5$ mm.

Table 1. Comparison of EMA and CMA for different ellipticity ratios.

Model	a (mm)	b (mm)	a/b	Theoretical f_L (MHz)	Simulated f_L (MHz)	First resonance f_L (MHz)	λ at f_L (mm)	$\frac{(a+b)}{\lambda}$
CMA	46	46	1.0	692	724	840	357.14	0.258
EMA1	48	44	1.1	670	701	804	373.13	0.247
EMA2	50.5	42	1.2	643	674	768	390.63	0.237
EMA3	53	40	1.33	618	649	736	407.61	0.228

2.2. Effect of ground plane size

Figure 3 displays the simulated return loss curves for different ground width W when other parameters are $L = 135mm$, $a = 52.5\ mm$, $b = 40\ mm$, $g = 0.5\ mm$, and ground length $L_g = 29.5\ mm$. It is seen in Figure 3 that the ground width has a great impact on the operating bandwidth. Variations in ground plane width shift the resonance positions unevenly and impedance matching may become worse. For proper impedance matching, an optimum ground plane width is required. When decreasing the width of the ground, the primary resonance shifts to the right, as illustrated in Table 2. We can note that as the overall width W changes from $180mm$ to $90mm$, the first resonance shifts slightly from 0.234λ to 0.282λ, but it has greater impedance matching. Thus, the optimal width of the ground plane is taken to be $W = 90mm$, which makes the structure compact.

Table 2. Changes in first resonance frequency for variation of ground plane width.

Ground plane width W(mm)	180	150	120	90
First resonance f_1 (MHz)	760	815	865	915
Wavelength λ at f_1 (mm)	394.74	368.10	346.82	327.87
$\frac{(a+b)}{\lambda}$	0.234	0.251	0.267	0.282

The ground plane width not only has a significant impact on the impedance bandwidth, but it is also effective on the radiation pattern characteristics. The H-plane copolarized patterns are almost omnidirectional for the antenna with different ground plane width. However, the cross-polarized pattern increases with larger ground plane width, as we can see from Figure 4. This is because the larger ground plane width introduces extra resonant modes, and the total radiated field is partially contributed by the increased current on the ground plane, which becomes significant for the cross-polarized patterns.

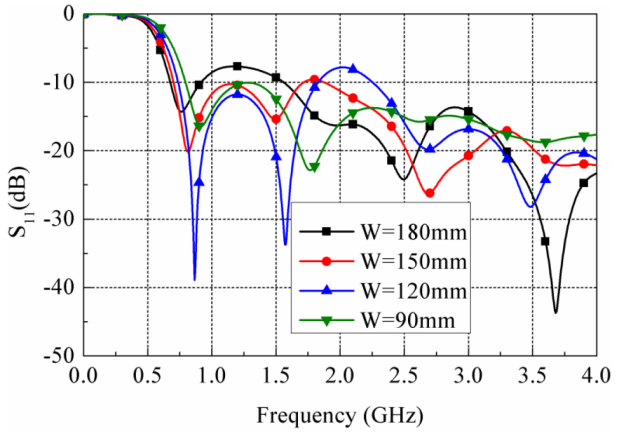

Figure 3. Simulated return loss curves for different values of ground width W.

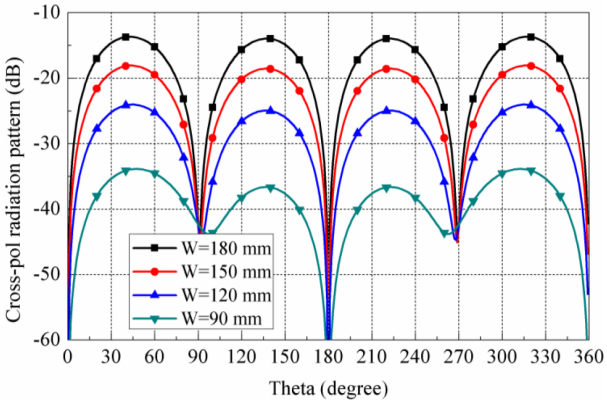

Figure 4. H-plane cross-polarized radiation patterns at 800 MHz for different values of ground plane width W.

3. DGS bandpass filter design

The bandpass DGS filter configuration and its resonance equivalent circuit are shown in Figures 5a and 5b, respectively. A DGS section can be replaced by a parallel LC resonator circuit, where the capacitance C_d and the inductance L_d of the equivalent circuit are expressed as [24]:

$$C_d = \frac{1}{2Z_0}\left[\frac{\omega_c}{(\omega_0^2 - \omega_c^2)}\right] \tag{2}$$

$$L_d = \frac{1}{\omega_0^2 C_d} \tag{3}$$

Here, $Z_0 = 50\Omega$ is the characteristic impedance of the microstrip line, ω_c is cut-off angular frequency at 3 dB, and ω_o is its angular pole frequency. A series capacitance C_g with the parallel resonance is created by coupling gap g in the 50Ω microstrip line just above the DGS slot and is taken as [24]:

$$C_g = \frac{1}{L_{eq}\omega_s^2} \tag{4}$$

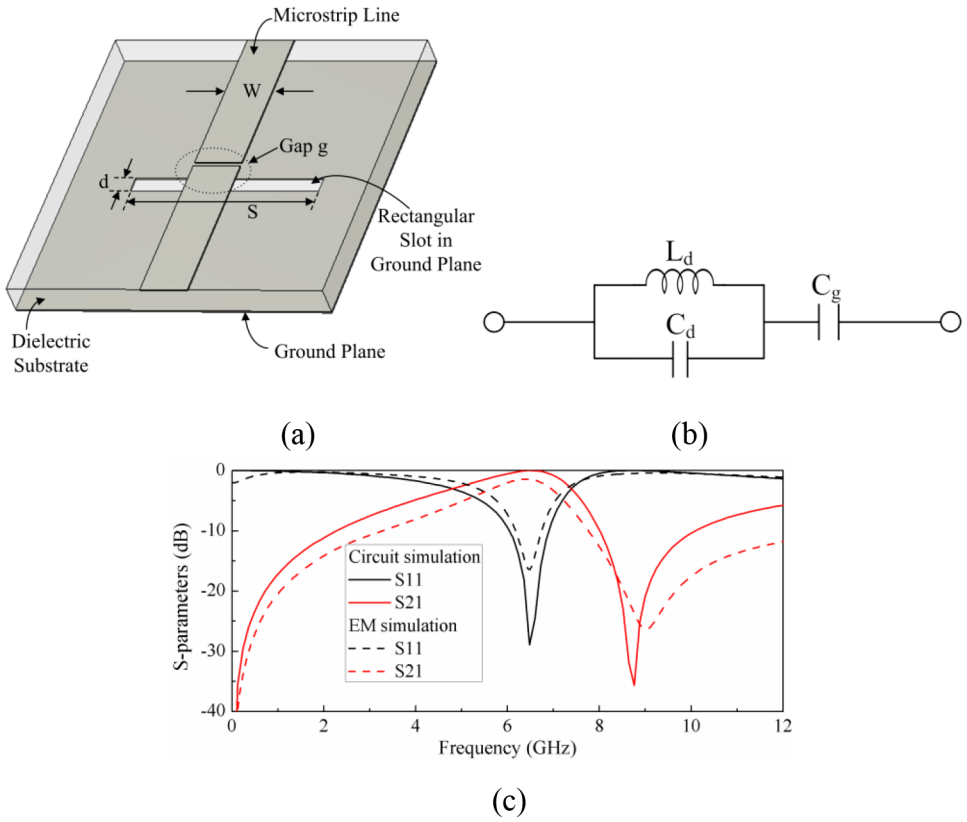

Figure 5. (a) Bandpass DGS filter, (b) equivalent circuit model, (c) S-parameters for bandpass DGS model.

Here, ω_s is angular resonance frequency, and equivalent inductance L_{eq} is obtained as:

$$L_{eq} = \frac{L_d}{\left[1 - \left(\frac{\omega_c}{\omega_0}\right)^2\right]} \tag{5}$$

The model shown in Figure 5a is simulated for DGS slot length S = 12 mm and width d = 1 mm. The microstrip line width W is taken at 3 mm with a coupling gap g = 0.2 mm. The circuit model values C_d = 0.276 pF, L_d = 1.21 nH, and C_g = 0.239 pF are obtained applying the above equations. The bandpass response of both the circuit simulator and EM simulator is closely matched, as shown in Figure 5c. If there is no coupling gap g presented in the model shown in Figure 5a, it will act as a band-stop filter.

4. Reconfigurable antenna design

To make the antenna reconfigurable, the elliptical disk is fed through the DGS integrated microstrip line, as shown in Figures 6a and 6b. The ellipse dimensions are taken to be the same as discussed previously. For impedance mismatching at higher frequencies, the ground plane below the feed line has been grooved at the edge, as indicated in Figure 6b. In the feed line of the proposed antenna model, six switches have been used, as indicated by SW in Figure 6. SW_3 and SW_4 are located p_1 distance away from SW_1, whereas SW_5 and SW_6 are positioned p_2 distance away from SW_1. The total DGS slot length is S and the gap between the radiator and ground plane is defined as c.

A prototype of the elliptical disk monopole antenna with optimal design, i.e. $L = 135mm$, $W = 90mm$, $a = 52.5mm$, $b = 40mm$, $g = 0.5mm$, $L_g = 29.5mm$, and $c = 0.5mm$, is fabricated and tested in the microwave lab, as shown in Figure 7. For the purpose of this experiment, band-switching from wideband to narrowband is done using adhesive copper bridges with a switch to represent the ON state that can be removed in the OFF state.

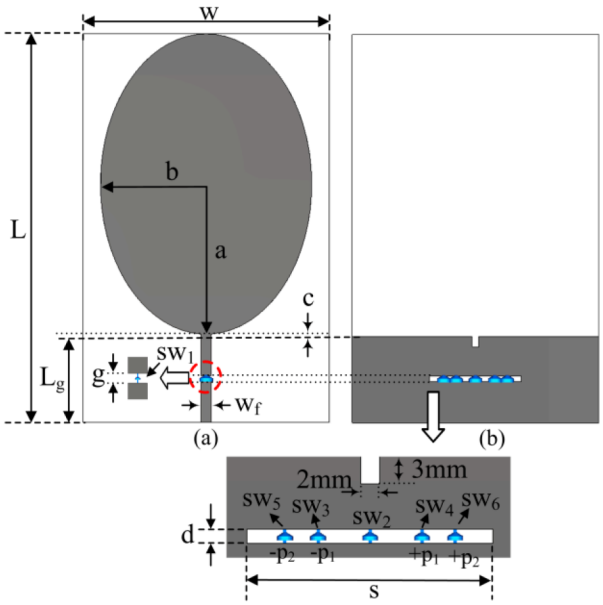

Figure 6. Proposed antenna model with six switches (indicated by SW): (a) front view, (b) bottom view.

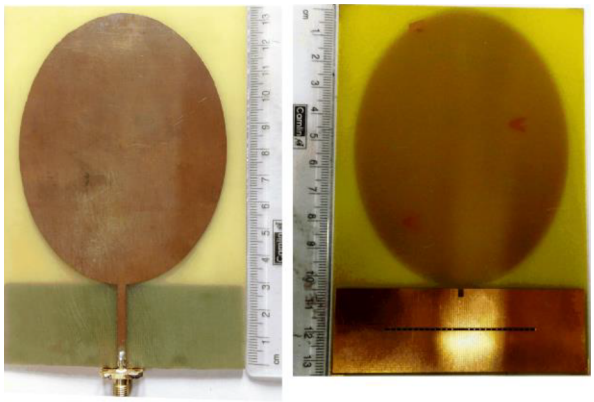

Figure 7. Fabrication prototype of elliptical monopole antenna.

Introducing a DGS filter model in the feed line of the ellipse, the UWB antenna can be reconfigured in different frequency bands. SW_3 and SW_4 are located $p_1 = 2.75$ mm away from SW_1, whereas SW_5 and SW_6 are positioned $p_2 = 4.5$ mm away from SW_1. The total slot length S is taken at 13 mm. When all the switches are in the ON state, the DGS has no impact on the feed line, and the antenna will operate in UWB mode (Band 1), giving a frequency range from 0.75 GHz to 13 GHz, as indicated in Figure 8. Thus, the antenna can be used for cognitive radio-sensing purposes that cover most of the useful frequency bands.

The antenna can be switched from UWB to narrowband mode by activating the DGS filter. When SW_1 is in the ON state and SW_2 is in the OFF state, the DGS acts as a band-stop filter. Depending on the other four switches, the band-stop position is fixed. Keeping SW_5 and SW_6 in the ON state and the other two switches in the OFF state, the effective slot length becomes 9 mm and gives a band-stop operation near 9 GHz. The lower frequencies pass easily through the DGS while blocking the higher frequencies, as shown in Figure 9.

When switches SW_1 and SW_2 are in the OFF state, the DGS will act as a bandpass filter and its resonance frequency can be tuned depending on other switch states. The resonance frequencies and corresponding switch states are provided in Table 3. The simulated and measured results are shown in Figure 10, where the antenna is tuned from 5 GHz to 12 GHz. In Table 3, –10 dB impedance bandwidths are provided, where the frequency band of 2.71–5.14 GHz is not covered in the narrowband mode. However, it can be seen from Figure 9 that the measured return loss is below –6 dB in the frequency band of 2.71–5.14 GHz. Hence, the antenna can operate effectively in narrowband mode at Band 2. Therefore, the proposed antenna is capable of tuning in the entire region of the sensed spectrum band from 0.75 GHz to 12 GHz. All the return loss is measured

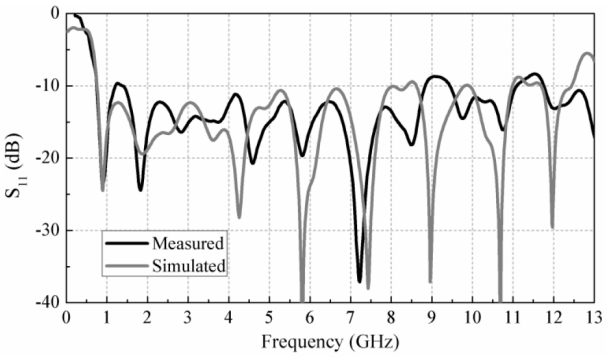

Figure 8. Return loss for sensing UWB monopole antenna.

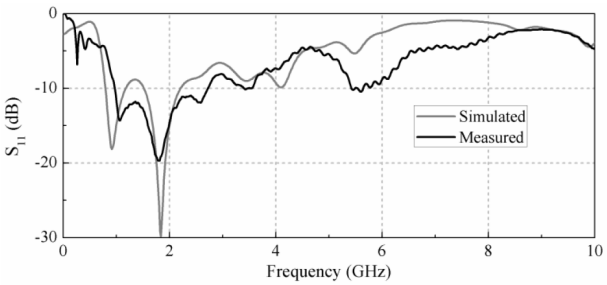

Figure 9. Return loss curves when DGS acts as a band-stop filter.

by using the Agilent Keysight PNA Network Analyzer N5221A (10 MHz to 13.5 GHz). The measured results reasonably match the simulation results. A minor discrepancy is due to fabrication tolerances.

Table 3. Proposed elliptical reconfigurable antenna-operating frequency bands.

Band	Switches						Frequency (GHz)	
	SW1	SW2	SW3	SW4	SW5	SW6	Simulation	Measured
1	ON	ON	ON	ON	ON	ON	0.76–12.43	0.75–13
2	ON	OFF	OFF	OFF	ON	ON	0.79–2.21	0.96–2.71
3	OFF	OFF	OFF	OFF	OFF	OFF	4.88–5.84	5.14–5.85
4	OFF	OFF	OFF	OFF	OFF	ON	5.99–6.54	5.68–6.17
5	OFF	OFF	OFF	OFF	ON	ON	6.52–7.73	6.25–7.92
6	OFF	OFF	OFF	ON	ON	ON	7.92–9.21	7.41–9.12
7	OFF	OFF	ON	ON	ON	ON	9.43–12.28	9.46–11.78

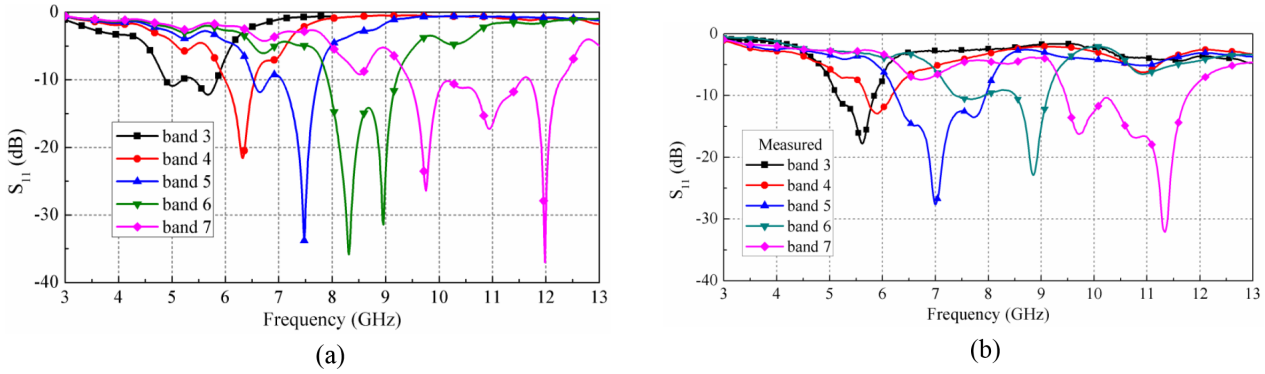

Figure 10. Return loss where DGS acts as a bandpass filter: (a) simulation results, (b) measured results.

As shown in Figure 11, low return loss (below –10 dB) always occurs over a wide frequency range when the real part of input impedance is matched to 50Ω and the imaginary part is not far from zero. In the proposed antenna input, real impedance varies slowly at the level of 50Ω, while reactance (imaginary part) remains small across an extremely wide frequency range, leading to UWB characteristics. The total radiation efficiency of the antenna is greater than 70% throughout the UWB operating region, as shown in Figure 12. Figure 13 shows that the group delay of the proposed antenna is almost constant (remains nearly 1 ns) in the entire UWB band, which indicates that the proposed antenna exhibits a linear transmission performance.

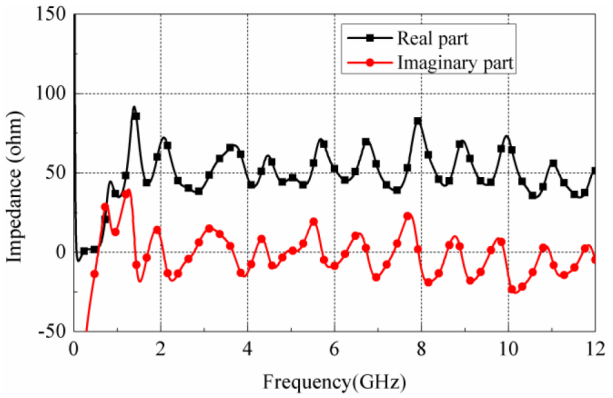

Figure 11. Input impedance curves of the proposed elliptical monopole antenna in UWB mode (Band 1).

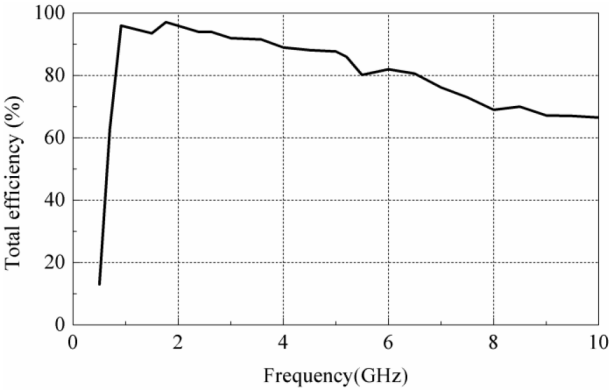

Figure 12. Total efficiency of the proposed antenna.

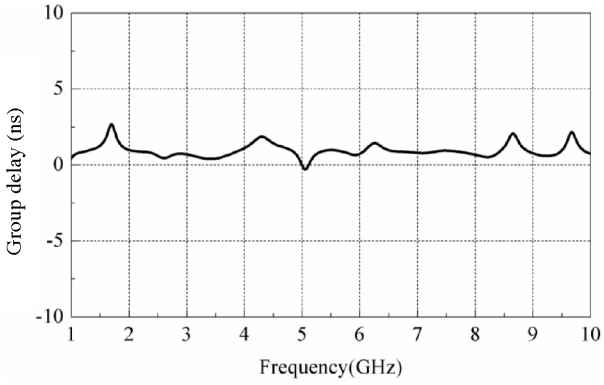

Figure 13. Group delay of the proposed antenna.

The simulated and measured radiation patterns close to the resonances at 0.915 GHz, 1.765 GHz, and 3.58 GHz are plotted in Figure 14. The measured radiation patterns are closely matched with the simulations. It is observed that E-plane (x-y plane) patterns have a large back lobe and resemble a doughnut, whereas the H-plane (y-z plane) pattern is omnidirectional. At higher mode resonances, this shape is slightly distorted. In the E-plane, the side lobe becomes smaller by splitting into minor ones, while the front lobes start to form humps and notches. At higher resonances, the H-plane radiation patterns show distortion, but still satisfy omnidirectionality, having less than 10 dB gain variation in all directions. Figure 15 plots the simulated and measured realized peak gain of the proposed elliptical monopole antenna. It is seen that the antenna has a satisfactory gain varying from 4 to 6 dB.

5. Conclusion

The current work has developed a prototype of a band reconfigurable elliptical disk monopole antenna operating from 750 MHz to 12 GHz in order to cover most licensed frequency bands. The antenna can operate at seven switchable states, including UWB state and six narrowband states. Tunability over such a wide frequency range has not been reported previously for planar monopole antennas. Omnidirectional radiation patterns and acceptable realized gain values make it extremely useful for wideband spectrum sensing as well as CR communication purposes.

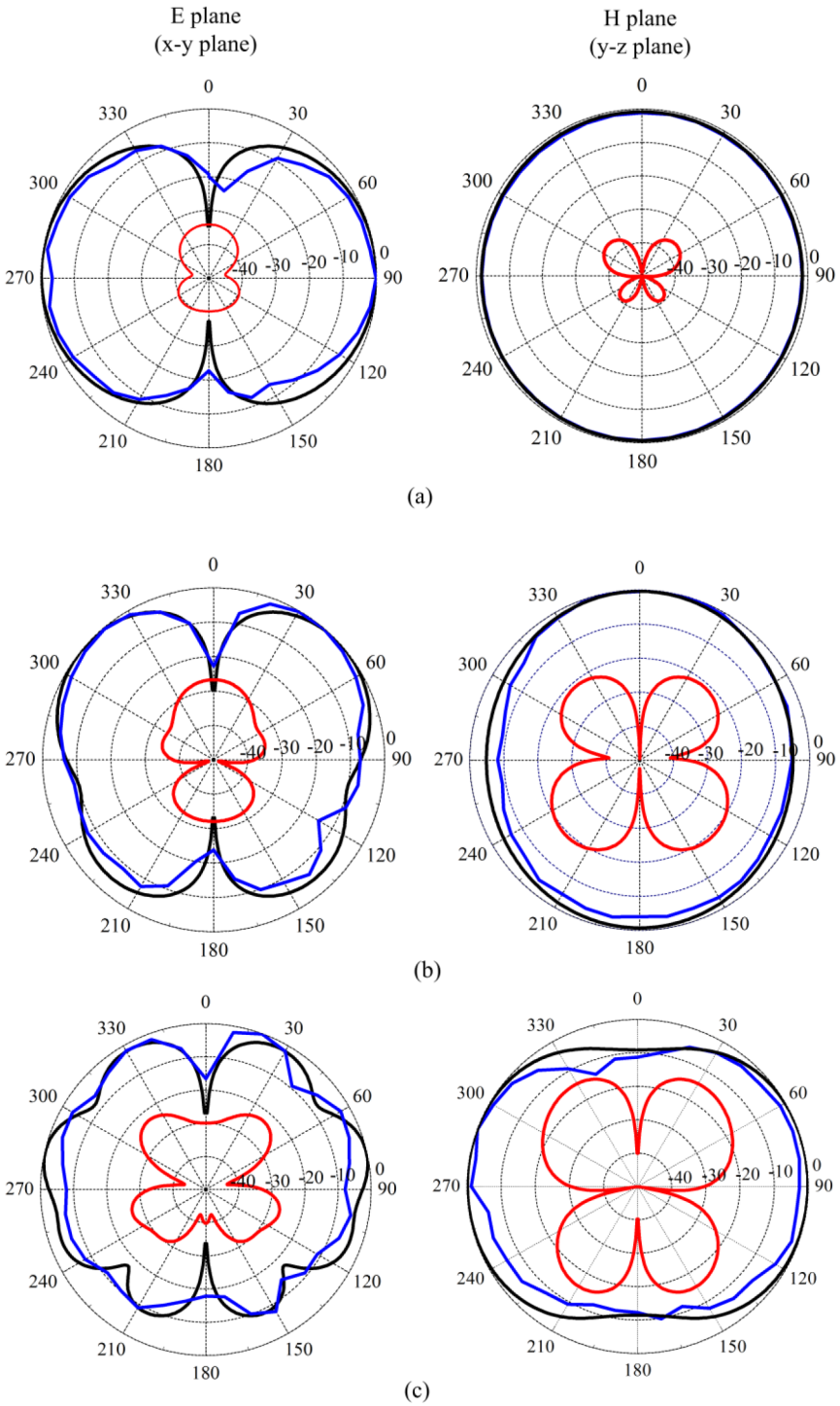

Figure 14. Copolarized measured (blue line), copolarized simulated (black line), and cross-polarized simulated (red line) radiation patterns of the proposed elliptical monopole antenna at (a) 0.915 GHz, (b) 1.765 GHz, and (c) 3.58 GHz.

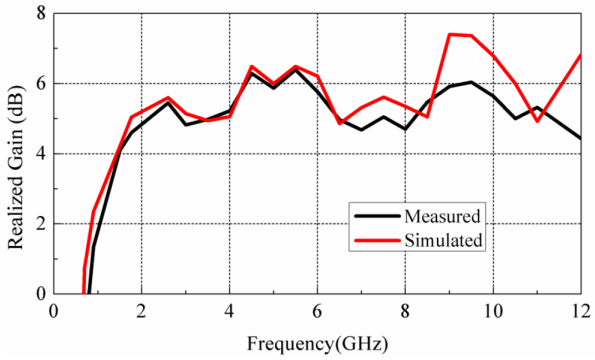

Figure 15. Realized gain of the elliptical monopole antenna.

References

[1] Rao PH. Antenna configurations for software defined radio and cognitive radio communication architecture. In: IEEE 2010 International Conference on Wireless Communication and Sensor Computing; 2–4 January 2010; Allahabad, India. New York, NY, USA: IEEE. pp. 1-4.

[2] Hussain R, Sharawi MS. A cognitive radio reconfigurable MIMO and sensing antenna system. IEEE Antenn Wirel Pr 2015; 14: 257-260.

[3] Thomas KG, Lenin N. Ultra wideband printed monopole antenna. Microw Opt Techn Lett 2007; 49: 1082-1085.

[4] Kelly JR, Hall PS, Song P. A reconfigurable wideband handset antenna operating from 460 MHz to 12 GHz. In: IEEE 2009 International Symposium on Antennas and Propagation Society; 1–5 June 2009; North Charleston, SC, USA. New York, NY, USA: IEEE. pp. 1-4.

[5] Gomez-Nunez E, Jardon-Aguilar H, Tirado-Mendez JA, Flores-Leal R. Ultra-wideband slotted disc antenna compatible with cognitive radio applications. Progr Electromagn Res Lett 2012; 34: 53-63.

[6] Hamid MR. Wideband reconfigurable antennas. PhD, University of Birmingham, Birmingham, UK, 2011.

[7] Ghanem F, Hall PS, Kelly JR. Two port frequency reconfigurable antenna for cognitive radios. Electron Lett 2009; 45: 534-535.

[8] Kelly JR, Song P, Hall PS, Borja AL. Reconfigurable 460 MHz to 12 GHz antenna with integrated narrowband slot. Pr Electromagn Res C 2011; 24: 137-145.

[9] Tawk Y, Costantine J, Avery K, Christodoulou CG. Implementation of a cognitive radio front-end using rotatable controlled reconfigurable antennas. IEEE T Antenn Propag 2011; 59: 1773-1778.

[10] Tawk Y, Costantine J, Hemmady S, Balakrishnan G, Avery K, Christodoulou CG. Demonstration of a cognitive radio front end using an optically pumped reconfigurable antenna system (OPRAS). IEEE T Antenn Propag 2012; 60: 1075-1083.

[11] Al-Husseini M, Tawk Y, Christodoulou CG, Kabalan KY, El-Hajj A. A reconfigurable cognitive radio antenna design. In: IEEE 2010 International Symposium on Antennas and Propagation Society; 11–17 July 2010; Toronto, ON, Canada. New York, NY, USA: IEEE. pp. 1-4.

[12] Al-Husseini M, Kabalan KY, El-Hajj A, Christodoulou CG. Reconfigurable microstrip antennas for cognitive radio. In: Kishk A, editor. Advancement in Microstrip Antennas with Recent Applications. Rijeka, Croatia: InTech, 2013. pp. 337-362.

[13] Kelly JR, Hall PS, Gardner P. Integrated wide-narrow band antenna for switched operation. In: IEEE 2009 European Conference on Antennas and Propagation; 23–27 March 2009; Berlin, Germany. New York, NY, USA: IEEE. pp. 3757-3760.

[14] Kelly JR, Hall PS. Reconfigurable slot antenna for Cognitive Radio applications. In: IEEE 2009 International Symposium of Antennas and Propagation Society; 1–5 June 2009; North Charleston, SC, USA. New York, NY, USA: IEEE. pp. 1-4.

[15] Jin GP, Zhang DL, Li RL. Optically controlled reconfigurable antenna for cognitive radio applications. Electron Lett 2011; 47: 948-950.

[16] Al-Husseini M, Ramadan A, El-Hajj A, Kabalan KY. A tunable filter antenna for cognitive radio systems. In: IEEE 2012 International Symposium on Antennas and Propagation Society; 8–14 July 2012; Chicago, IL, USA. New York, NY, USA: IEEE. pp. 1-2.

[17] Al-Husseini M, Ramadan A, Zamudio ME, Christodoulou CG, El-Hajj A, Kabalan KY. A UWB antenna combined with a reconfigurable bandpass filter for cognitive radio applications. In: IEEE 2011 Topical Conference on Antennas and Propagation in Wireless Communications; 12–16 September 2011; Torino, Italy. New York, NY, USA: IEEE. pp. 902-904.

[18] Ramadan AH, Costantine J, Al-Husseini M, Kabalan KY, Tawk Y, Christodoulou CG. Tunable filter-antennas for cognitive radio applications. Prog Electromagn Res B 201; 57: 253-265.

[19] Aboufoul T, Alomainy A, Parini C. Reconfiguring UWB monopole antenna for cognitive radio applications using GaAs FET switches. IEEE Anten Wirel Pr 2012; 11: 392-394.

[20] Ghanem F, Kelly JR, Hall PS. Switched UWB to narrowband planar monopole antenna. In: IEEE 2010 European Conference on Antennas and Propagation; 12–16 April 2010; Barcelona, Spain. New York, NY, USA: IEEE. pp. 1-3.

[21] Boudaghi H, Azarmanesh M, Mehranpour M. A frequency-reconfigurable monopole antenna using switchable slotted ground structure. IEEE Antenn Wirel Pr 2012; 11: 655-658.

[22] Koley S, Bepari D, Mitra D. Band-reconfigurable monopole antenna for cognitive radio applications. IETE J Res 2015; 61: 411-416.

[23] Kumar G, Ray KP. Broadband Microstrip Antennas. Norwood, MA, USA: Artech House, 2003.

[24] Yoon JS, Kim JG, Park JS, Park CS, Lim JB, Cho HG, Kang KY. A new DGS resonator and its application to bandpass filter design. In: IEEE 2004 International Microwave Symposium Digest; 6–11 June 2004; Fort Worth, TX, USA. New York, NY, USA: IEEE. pp. 1605-1608.